Internal Medicine
The Japanese Society of Internal Medicine
doi: 10.2169/internalmedicine.2116-18
Intern Med 58: 1217-1224, 2019
http://internmed.jp

【 ORIGINAL ARTICLE 】

Decreased Mean Kurtosis in the Putamen is a Diagnostic Feature of Minimal Hepatic Encephalopathy in Patients with Cirrhosis

Takuro Sato[1], Kei Endo[1], Keisuke Kakisaka[1], Yuji Suzuki[1], Yohei Kooka[1], Kei Sawara[1], Kenji Ito[2], Makoto Sasaki[2] and Yasuhiro Takikawa[1]

Abstract:

Objective To prevent the development of overt hepatic encephalopathy, the early intervention for minimal hepatic encephalopathy (MHE) based on an accurate diagnosis is essential. This study investigated whether or not magnetic resonance diffusion kurtosis imaging (DKI) and diffusion tensor imaging (DTI) could detect brain microstructure abnormalities in MHE. The aim was to confirm whether or not brain microstructure abnormalities detected by magnetic resonance (MR) imaging could be used for the diagnosis of MHE.

Methods Thirty-two subjects were prospectively examined with a 3-T MR scanner. Tract-based spatial statistics and region of interest analyses of diffusion imaging were performed to compare the mean kurtosis (MK), fractional anisotropy (FA), and mean diffusivity (MD) values between patients with and without minimal hepatic encephalopathy. The diagnostic performance for the detection of MHE was assessed with a receiver operating characteristic analysis.

Results Ten subjects were diagnosed with MHE by neuropsychological testing. After the exclusion of unsuitable subjects, we analyzed 9 subjects with MHE and 14 without MHE. The patients with MHE had a reduced MK in the widespread white matter. We also found significant decreases in the MK in the caudate nucleus, putamen, globus pallidus, and/or thalamus in the subjects with MHE. The MK in the putamen showed the best diagnostic performance for differentiating the subjects with MHE from those without MHE (cut-off value, 0.74; sensitivity, 0.89; specificity, 0.86).

Conclusion DKI detects changes in the cerebral white matter and basal ganglia regions of patients with MHE more sensitively than DTI. The MK values in the putamen can be a useful marker for diagnosing MHE from cirrhotic patients without MHE.

Key words: diffusion kurtosis imaging, DKI, minimal hepatic encephalopathy, putamen

(Intern Med 58: 1217-1224, 2019)
(DOI: 10.2169/internalmedicine.2116-18)

Introduction

Hepatic encephalopathy (HE) is a neuropsychiatric and cognitive disorder that occurs due to decompensated cirrhosis (1). Symptomatic HE is termed 'overt' HE and reduces the quality of life while increasing the mortality in patients with cirrhosis (2). Minimal hepatic encephalopathy (MHE) increases the risk of progression to overt HE (3). Since symptoms of MHE comprise attention and visuo-motor coordination deficits, sensitive examination methods that assess psychometric performance are required to identify this condition (4, 5). Thus, MHE is defined as a condition characterized by subtle abnormalities that can be detected only using specific neuropsychometric and/or neurophysiological tools in cirrhosis patients with otherwise normal neurological examination results (4).

For the accurate diagnosis of MHE, the following pa-

[1]Division of Hepatology, Department of Internal Medicine, Iwate Medical University, Japan and [2]Division of Ultrahigh Field MRI, Institute for Biomedical Sciences, Iwate Medical University, Japan
Received: September 11, 2018; Accepted: October 21, 2018; Advance Publication by J-STAGE: January 10, 2019
Correspondence to Dr. Keisuke Kakisaka, keikaki@iwate-med.ac.jp

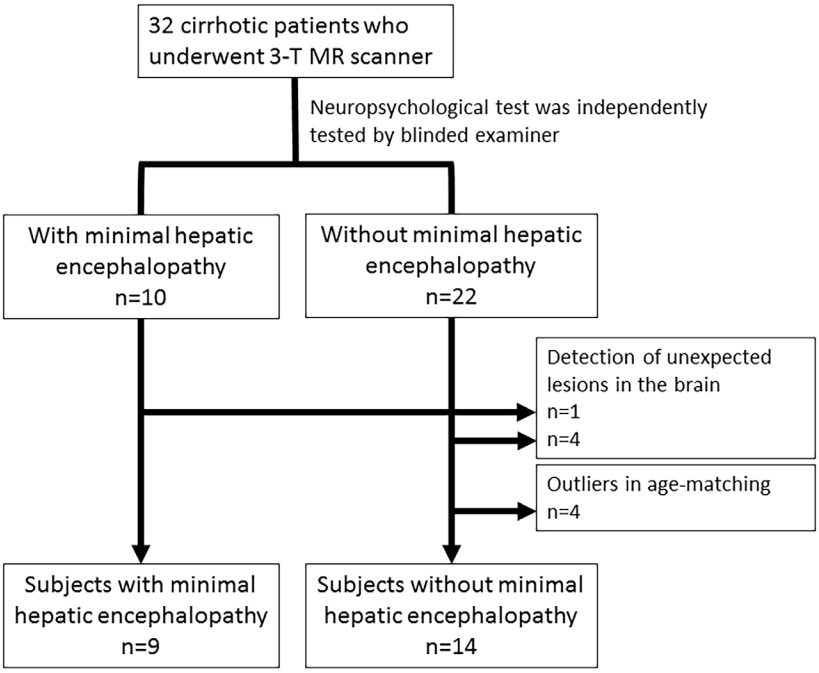

Figure 1. **Flow chart of the study design.**

rameters need to be evaluated: 1) the quality of life; 2) mental state; 3) results of neuropsychological testing (NPT); and 4) disorders of speech and cognition. However, it is difficult to perform such a comprehensive diagnosis in routine clinical practice. As an accurate diagnosis of MHE is essential for improving the prognosis of patients with cirrhosis, objective and repeatable examination methods for the diagnosis of MHE need to be established.

Recently, metabolic disturbances in the brain of patients with MHE were identified using 3.0 Tesla magnetic resonance imaging (MRI) (6). That article reported increases in the glutamine levels and reductions in the myo-inositol levels in the brain of patients with MHE. Since myo-inositol controls the increase in the osmotic pressure due to increased glutamine via ammonia metabolism in the brain, these changes were considered to be the result of a buffering response in order to maintain the intracellular osmotic pressure. These findings and those of previous reports suggest that astrocytes in MHE might become edematous. Thus, diffusion MRI may be useful for detecting increases in the water component of the brain in patients with MHE.

Diffusion tensor imaging (DTI) is an advanced MR technique that is widely used to quantify the diffusivity and/or anisotropy of water diffusion. DTI parameters include the mean diffusivity (MD), which measures the average diffusivity of water, and fractional anisotropy (FA), which measures the degree of directionality of diffusion. Increased MD and/or decreased FA have been reported in patients with MHE (7-9). Recently, the concept of diffusion kurtosis imaging (DKI), which can detect minute histological changes in complex brain structures by quantifying the degree of non-Gaussian water diffusion, has been proposed (10). Previous studies have suggested that DKI is more sensitive to microstructural changes in various neurological disorders than DTI (11-13). Indeed, the usefulness of the mean kurtosis (MK), a parameter calculated from DKI data, has been reported in studies of several diseases, including Parkinson's disease, multiple sclerosis, and migraine (14-16). Although previous studies have established objective findings that can aid in the diagnosis of MHE using MRI (7, 9, 17, 18), these studies were based on a comparison of patients with MHE and healthy controls. For example, DKI revealed microstructural changes in patients with cirrhosis compared with healthy controls (19), suggesting that cirrhosis itself affects DKI. As such, the microstructural changes detected by DKI in previous studies may only show changes due to cirrhosis.

Whether or not DKI/DTI can identify abnormalities in the brain microstructure of MHE patients compared with those of cirrhosis patients without MHE remains unclear. We therefore compared the DKI/DTI findings among cirrhosis patients with and without MHE.

Materials and Methods

Subjects

For this study, 32 subjects who underwent MRI were prospectively registered after providing their written informed consent from March 2013 to September 2017 (Fig. 1). The inclusion criteria were as follows: 1) a diagnosis of liver cirrhosis based on the clinical presentation, routine laboratory data, and imaging; and 2) age 18-80 years. The exclusion criteria included a history of mental disorder and overt HE of West Haven Criteria grade 1 or greater.

All protocols reported in this paper were approved by the Institutional Review Board of Iwate Medical University and

were performed in accordance with the requirements of the Declaration of Helsinki (64th WMA General Assembly, Fortaleza, Brazil, October 2013).

The diagnosis of MHE

To diagnose MHE, NPT was performed using a specific application on a mobile tablet (20). The NPT comprises four tests: the number connection tests A and B, the digit symbol test, and the block design test. When patients exhibited abnormalities for two or more tests in NPT, they were diagnosed with MHE (MHE group); those that did not have a diagnosis of MHE were classified into the non-MHE group.

MR image acquisition

MRI was performed using a 3.0-Tesla scanner (Discovery MR750, GE Healthcare, Milwaukee, USA) with an 8-channel head coil. DKI/DTI source images were obtained using a single-shot spin-echo echo-planar imaging technique with the following scanning parameters: repetition time/echo time 4,000/110 ms; motion-probing gradients, 20 directions with a duration of 31.0 ms and a separation of 39.8 ms; b values 0, 1,000, and 2,500 s/mm^2; field of view 22 cm; matrix size 128×128; reconstructed matrix size 256×256; slice thickness 3.0 or 4.0 mm without gaps; and acquisition time 10 minutes 12 seconds, which were optimised in a previous report (21) and used in other reports (11, 16, 22). Conventional MR images, including axial T1- and T2-weighted images, were also obtained.

Analyses of imaging data

One of the authors (K.I.), who had been blinded to the clinical presentation of the subjects, performed all of the imaging analyses. Diffusion metric maps, such as mean kurtosis (MK), fractional anisotropy (FA), and mean diffusivity (MD), were calculated using in-house software and used in previous studies (11, 16, 21, 22). In this study, the FA and MD values were calculated using only the DTI data from *b*-values of 0 and 1,000 s/mm^2.

To identify changes in the white matter (WM) of the patients with MHE, we carried out voxel-wise statistical analyses of the MK, FA, and MD maps for screening the whole brain using tract-based spatial statistics (TBSS) implemented in FSL 5.0.9 (FMRIB, Oxford. http://www.fmrib.ox.ac.uk/fsl/) (23). After skull stripping, all subjects' FA maps were aligned into FMRIB58-FA standard space using FMRIB's Non-linear Image Registration Tool. The mean FA image of each subject was created and then thinned and thresholded at FA >0.20 to generate a mean FA skeleton that represented the canters of major WM tracts common to all subjects. The mean FA skeleton was also masked to extract only the cerebral WM using the Harvard-Oxford Subcortical Structural Atlas implemented in FSL. The FA map of each subject was then projected onto this skeleton to obtain skeleton FA maps. MK and MD maps were also projected onto the mean FA skeleton by applying the same transformation as that for the FA map.

A voxel-wise comparison of the MK, FA, and MD values was performed between patients in the MHE and non-MHE groups. The threshold for statistical significance was p<, using threshold-free cluster enhancement (TFCE) with family-wise effort (FWE) correction for multiple comparison corrections (corrected $p<0.05$, 5,000 permutations). We also calculated the ratio of the areas of significant changes in MK, FA, and MD to the mean FA skeleton area. To perform region-of-interest (ROI) analyses in the cerebral WM skeleton, the ROI masks drawn on the mean FA skeleton were transformed into each native space following the back-projection procedure in TBSS. The mean MK, FA, and MD values of the WM were automatically measured using the coregistered ROI.

To perform ROI analyses in the basal ganglia, the Johns Hopkins University (JHU) Eve atlas was warped to the native space of each subject using the inverse transformation matrices that were obtained by the registration of the FA and b0 maps into the corresponding maps of the JHU-Eve atlas via methods similar to those described in a previous study (11). The mean MK, FA, and MD values of the caudate nucleus (CN), putamen (Put), globus pallidus (GP), and thalamus (TH) were then automatically measured using coregistered ROIs.

Child-Pugh score and model of end-stage liver disease (MELD)

Child-Pugh scores were calculated using data on prothrombin time international ratio (PT-INR), serum albumin levels (Alb), total bilirubin (T-Bil), and the presence of encephalopathy and ascites. Child-Pugh classifications were defined as class A (5-6), class B (7-9), and class C (10-15). The MELD score was calculated using the following formula, based on the results of a haematological examination: MELD=9.57 loge [Cre (mg/dL)] +3.78 loge [T-Bil (mg/dL)] +11.20 loge (PT-INR) +6.43.

Laboratory data

Plasma PT-INR and serum levels of Alb, alanine aminotransferase, ammonia (NH_3), aspartate aminotransferase, and creatinine, as well as the platelet count and T-Bil, were determined by an autoanalyzer (JCA-BM2250; JEOL, Tokyo, Japan).

Statistical analyses

Statistical analyses were performed using the SPSS 17.0 software program (SPSS, Chicago, USA). Continuous variables are presented as the mean±standard deviation. Either the Mann-Whitney *U* test or Fisher's exact test was used for the comparison of the MK, FA, and MD values obtained by the ROI analysis as well as to compare the demographics between the patients in the MHE and non-MHE groups. The diagnostic performance for detection of MHE using DKI/DTI was assessed using the receiver operating characteristics (ROC) method. The cut-off values of MK, FA, and MD for MHE were estimated using the area under the ROC

Table 1. Demographic and Clinical Characteristics of the MHE and Non-MHE Groups.

	MHE	non-MHE	p value
Sex (M:F)	5:4	12:2	0.108
Age	63.1±9.8	58.9±6.6	0.233
Aetiology			
Alcohol	4	7	
HCV	3	3	
NASH	2	4	
Alb	3.6±0.4	3.7±0.6	0.763
Cre	1.1±0.8	0.7±0.2	0.179
AST	53±21	39±16	0.091
ALT	40±21	28±9	0.088
T-Bil	1.6±0.8	1.1±0.8	0.201
NH_3	111±53	75±28	0.046
Plt	92±42	141±78	0.101
PT (s)	14.6±2.2	15.0±3.3	0.788
PT-INR	1.21±0.18	1.23±0.27	0.860
MELD	8.8±3.6	5.2±4.0	0.035
Child-Pugh score (A:B)	4:5	8:6	0.584

ALT: alanine aminotransferase, AST: aspartate transaminase, Cre: creatinine, HCV: hepatitis C virus infection, MHE: minimal hepatic encephalopathy, MELD: model of end-stage liver disease, NASH: non-alcoholic steatohepatitis, Plt: platelet count, PT: prothrombin time, PT-INR: prothrombin time-international normalised ratio, T-Bil: total bilirubin

(AUROC) and was calculated using the maximum point of the Youden index (sensitivity+specificity-1). For all statistical analyses, a level of significance of $p<0.05$ was used.

Results

Characteristics of the subjects in the MHE and non-MHE groups

Of the 32 subjects evaluated, 10 were classified into the MHE group and 22 into the non-MHE group (Fig. 1). After classification of the subjects based on the MHE diagnosis, we excluded 5 due to the detection of unexpected lesions in the brain (1 from the MHE group and 4 from the non-MHE group). We excluded another four subjects from the non-MHE group due to outliers in age-matching between the groups. After the exclusion of these subjects, we ultimately analysed 9 MHE subjects and 14 non-MHE subjects. The detailed characteristics of these 23 subjects are summarized in Table 1.

With regard to the aetiology of liver cirrhosis, alcohol consumption, HCV, and non-alcoholic steatohepatitis were the etiological factors in 4, 3, and 2 patients in the MHE group and 7, 3, and 4 patients in the non-MHE group, respectively. When laboratory data were compared between the two groups, the NH_3 level and MELD score in the MHE group showed significant differences from those in the non-MHE group (111 μg/dL vs. 53 μg/dL and 8.8 vs. 5.2, respectively).

The MK using DKI and FA using DTI were decreased in the WM in the subjects with MHE

Fig. 2 shows the results of the voxel-wise group analysis using TBSS. Compared with the non-MHE patients, the MK and FA values of the WM in the patients with MHE were significantly decreased in the widespread WM, whereas the MD values were significantly increased around only the left frontal and right occipital regions. Compared with the FA and MD, MK detected the broadest area with significant changes in the patients with MHE (MK, 54.8%; FA, 34.3%; MD, 4.0%, respectively) (Fig. 2). Regarding the ROI analysis, the MK and FA values of the WM were significantly lower and the MD values significantly higher in the MHE group (0.91, 0.43, and 0.83, respectively) than in the non-MHE group (0.95, 0.45, and 0.80, respectively) ($p=0.005$, 0.024, and 0.039, respectively) (Fig. 3).

The MK using DKI and FA using DTI detected decreasing changes at the basal ganglia in the subjects with MHE

Fig. 4 shows representative DKI/DTI images of the MHE and non-MHE subjects. The MK values in the Put and GP were markedly decreased in the MHE patients, while the FA values were only slightly decreased. There were no substantial differences in the MD between the groups.

Regarding the ROI analysis in the basal ganglia, the MK values of the CN, Put, GP, and TH were significantly lower in the MHE group (0.57, 0.70, 0.83, and 0.73, respectively) than in the non-MHE group (0.60, 0.77, 0.90, and 0.77, re-

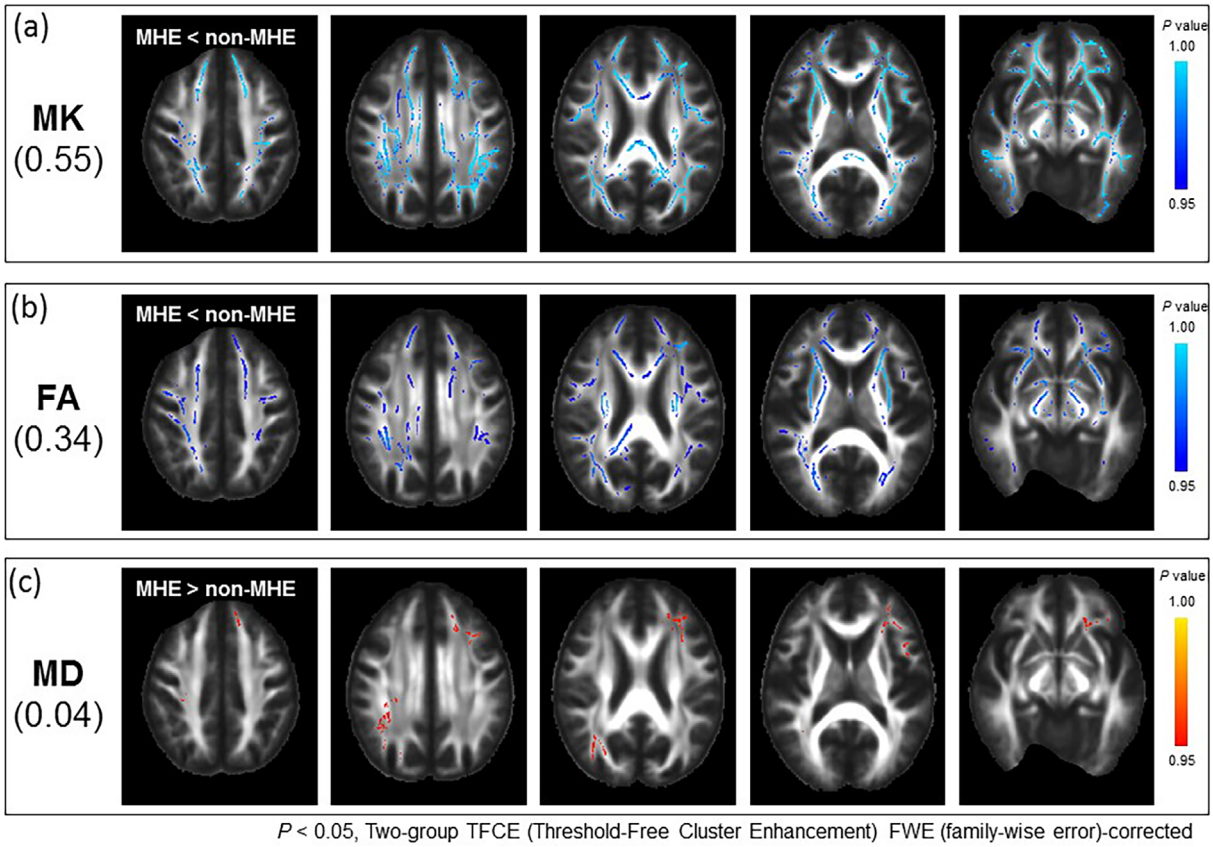

Figure 2. **Voxel-wise statistical analyses of the mean kurtosis (MK), fractional anisotropy (FA), and mean diffusivity (MD) using tract-based spatial statistics. a, b, and c: Each panel shows the region with a significant change detected by each method (a: MK, b: FA, or c: MD, respectively). Clusters that survived FWE correction of p<0.05 with TFCE are presented as a coloured area showing a significant change in the white matter. To present differences in the MK, FA, and MD in the areas with significant changes, coloured regions indicating skeletal lesions for MK, FA, and MD are demonstrated. FWE: family-wise effort, TECE: threshold-free cluster enhancement**

spectively) (p=0.036, 0.002, 0.005, and 0.023, respectively) (Fig. 3a). Similarly, the FA values of the CN, Put, and GP were also significantly lower in the MHE group (0.15, 0.19, and 0.29, respectively) than in the non-MHE group (0.16, 0.21, and 0.32, respectively) (p=0.012, 0.002, and 0.0001, respectively) (Fig. 3b). In contrast, the MD values in the basal ganglia showed no marked differences between the groups (Fig. 3c).

The MK in the putamen was useful for distinguishing patients with MHE among subjects with liver cirrhosis

ROC analyses performed for the MK, FA, and MD values of the CN, Put, GP, TH, and WM revealed significant differences between the groups (Table 2). Among the metrics, the MK values of the Put achieved an AUROC of 0.90, and the sensitivity, specificity, positive predictive value (PPV), and negative predictive values were more than 80% (0.89, 0.86, 0.80, and 0.92, respectively) between the MHE and non-MHE groups. The AUROC value of FA in the GP was the highest at 0.91, while the PPV of FA in the GP was lower than that of MK in the Put (0.69 vs. 0.80).

Discussion

In this study, we compared the DKI/DTI findings between cirrhosis patients with and without an MHE diagnosis in order to identify abnormalities in the brain microstructure that are diagnostic for MHE. The significant findings of the present study are as follows: 1) MRI-derived parameters of water component in WM and basal ganglia showed changes in relation to the development of MHE, 2) these changes were clearly detected by MK, and 3) Put on MK imaging was a diagnostic finding of MHE. According to these results, MHE can be diagnosed objectively and repeatedly by evaluating MK using MRI.

The accurate diagnosis of MHE is important because MHE is considered to precede overt HE and thus is associated with a reduction in both the quality of life and activity of daily life (24). Since several papers have reported the effectiveness of several agents for the treatment of HE (25, 26), MHE must be diagnosed with the appropriate timing. Diagnostic methods for MHE include specific neuropsychometric and/or neurophysiological examinations,

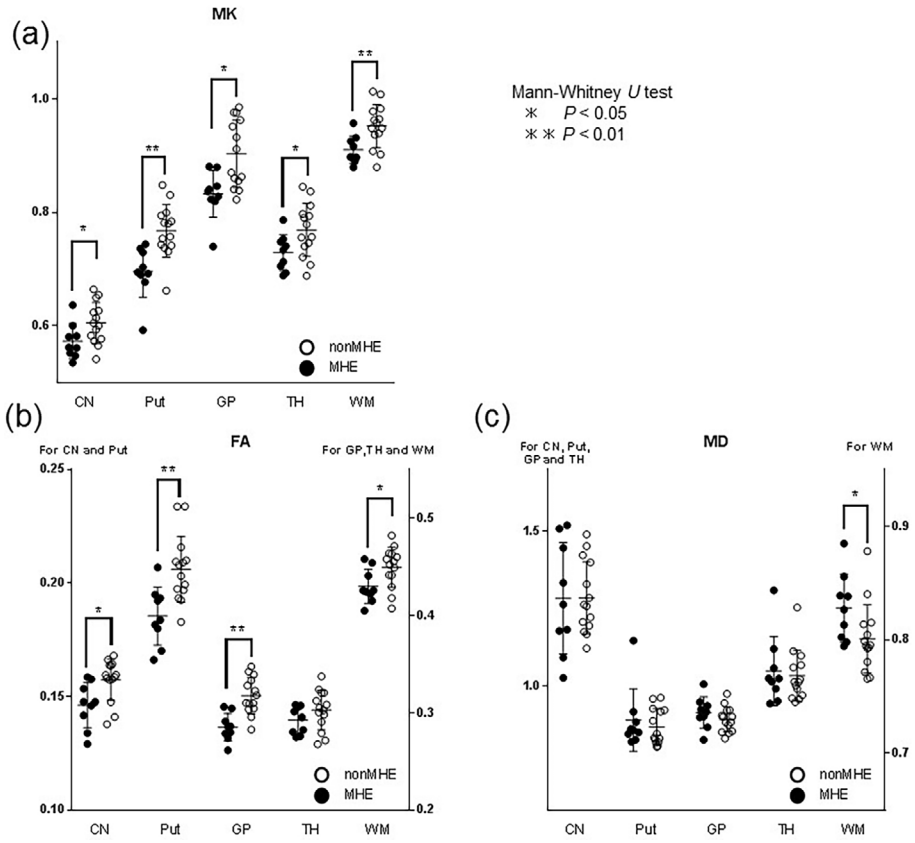

Figure 3. **The mean kurtosis (MK), fractional anisotropy (FA), and mean diffusivity (MD) of the basal ganglia and white matter (WM) were compared between the two groups. a, b, and c: The caudate nucleus (CN), putamen (Put), globus pallidus (GP), thalamus (TH), and WM were evaluated using ROI analyses to assess the MK (a), FA (b), and MD (c) values. The vertical axis indicates the intensity of each imaging analysis. Closed and open circles indicate the minimal hepatic encephalopathy (MHE) group and non-MHE group, respectively. The horizontal axis indicates the region selected for the analysis. Significant differences between the two groups were analysed using the Mann-Whitney *U* test. Single asterisks (*) and double asterisks (**) indicate p<0.05 and p<0.01, respectively.**

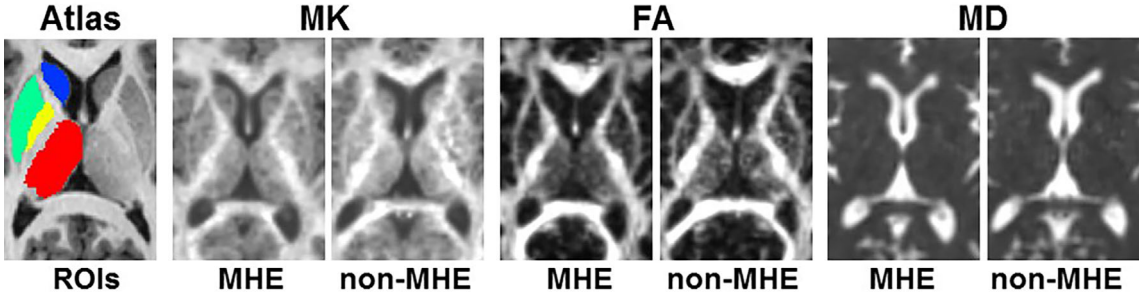

Figure 4. **Diffusion kurtosis and tensor maps of representative minimal hepatic encephalopathy (MHE) and non-MHE patients and the regions-of-interest (ROI) of the basal ganglia structures. The MHE patient was a 63-year-old woman, and the non-MHE patient was a 58-year-old man. The atlas-based ROIs of the right caudate nucleus (blue), putamen (green), globus pallidus (yellow), and thalamus (red) are shown on the Johns Hopkins University Eve T1-weighted images. The mean kurtosis (MK) is substantially decreased in the putamen and globus pallidus of the patient with MHE, while the fractional anisotropy (FA) is only slightly decreased. No marked changes in the mean diffusivity (MD) were observed in the patient with MHE compared with the non-MHE patient.**

such as NPT. However, these tests are time-consuming for outpatients. To ensure that appropriate intervention is provided following an accurate diagnosis of MHE, repeatable and objective diagnostic methods are required. According to

Table 2. Accuracy of DKI/DTI Parameters for Diagnosis of Minimal Hepatic Encephalopathy among Cirrhotic Patients.

	AUROC	Cut-off	Sensitivity	Specificity	PPV	NPV
MK_WM	0.84	0.93	0.89	0.79	0.73	0.92
MK_CN	0.76	0.58	0.78	0.71	0.64	0.83
MK_Put	0.90	0.74	0.89	0.86	0.80	0.92
MK_GP	0.83	0.85	0.78	0.79	0.70	0.85
MK_TH	0.76	0.75	0.89	0.64	0.62	0.90
FA_WM	0.79	0.44	0.78	0.79	0.70	0.85
FA_CN	0.80	0.15	0.78	0.79	0.70	0.85
FA_Put	0.88	0.19	0.89	0.79	0.73	0.92
FA_GP	0.91	0.31	1.00	0.71	0.69	1.00
MD_WM	0.76	0.80	0.89	0.57	0.57	0.89

DKI/DTI: diffusion kurtosis imaging/diffusion tensor imaging, AUROC: area under the receiver operating characteristics, PPV: positive predictive value, NPV: negative predictive value, MK: mean kurtosis, WM: white matter, CN:caudate nucleu, Put: putamen, GP: globus pallidus, TH: thalamus, FA: fractional anisotropy, MD: mean diffusivity

our results, subtle changes in the basal ganglia and WM can be detected by evaluating MK and are useful for the accurate diagnosis of MHE. Of note, these findings are objective, and examinations using DKI/DTI are repeatable.

The present study was designed to perform a comparison among patients with cirrhosis; however, previous studies that have shown the utility of the MD for the diagnosis of MHE by comparing healthy controls and subjects with MHE (7, 9, 18). Importantly, it has been reported that the MR features of the brain microstructure in patients with cirrhosis are different from those in healthy controls (19). However, given that the patients in both the non-MHE and MHE groups had liver cirrhosis in the present study, our findings in the MHE group could be attributed to MHE rather than liver cirrhosis. We therefore propose that these findings are useful for the diagnosis of MHE. Recently, the blood flow in the Put as evaluated by functional MRI was found to be changed in MHE patients when compared to those without MHE (27). We considered that this result supported our findings of oedematous changes in the Put in MHE patients.

The pathophysiology of HE is hypothesised to involve swelling of the astrocytes due to an imbalance in amino acid metabolism. Indeed, we have previously shown increases in glutamine levels detected by MR spectroscopy in patients with MHE (6). The grey matter of the brain contains the cell bodies of neurons and many kinds of glial cells (28), which explains the observations of changes in the DTI signal in the grey matter due to the presence of oedematous cells in patients with MHE (9, 17). However, given that previous studies compared patients with MHE and healthy controls, the findings in those studies might have been different had a comparison been performed among patients with liver cirrhosis or portal hypertension. In the present study, DKI clearly revealed changes in the signal in a broad area of the WM, indicating that the WM had been affected by MHE.

The PPVs of the MK in the Put and the FA in the GP were 0.80 and 0.69, respectively. The PPV is the probability that subjects with a positive test actually have the disease. A high PPV increases the probability that the subject has the disease. Because we focused on establishing objective and reproducible methods for diagnosing MHE, we therefore concluded that Put in MK was useful for the diagnosis of MHE in this study.

One particular limitation associated with the present study warrants mention. Owing to the cross-sectional design of the present study, the repeatability of the observations may be low. Although previous studies have reported that findings detected by MRI in subjects with MHE are reversible (7), the reversibility of the findings we noted in this study remains unclear. To further clarify the pathophysiology of MHE, larger serial-observation studies of the MRI findings of patients with MHE are warranted.

The present study revealed that brain microstructural changes in MHE can be detected by evaluating MR images. The MK value can be useful for objectively detecting subtle changes in the Put in MHE patients, and these findings are diagnostic for MHE in patients with cirrhosis.

The authors state that they have no Conflict of Interest (COI).

Financial Support

This study was supported by a Grant-in-Aid for Strategic Medical Science Research (S1491001) from MEXT of Japan and JSPS KAKENHI (grant number JP18K07980 for KK and JP15K 19346 for KS).

References

1. Wijdicks EF. Hepatic encephalopathy. N Engl J Med **375**: 1660-1670, 2016.
2. Fichet J, Mercier E, Genee O, et al. Prognosis and 1-year mortality of intensive care unit patients with severe hepatic encephalopathy. J Crit Care **24**: 364-370, 2009.
3. Romero-Gomez M, Grande L, Camacho I, Benitez S, Irles JA, Castro M. Altered response to oral glutamine challenge as prognostic factor for overt episodes in patients with minimal hepatic

encephalopathy. J Hepatol **37**: 781-787, 2002.
4. Stewart CA, Smith GE. Minimal hepatic encephalopathy. Nat Clin Pract Gastroenterol Hepatol **4**: 677-685, 2007.
5. Wein C, Koch H, Popp B, Oehler G, Schauder P. Minimal hepatic encephalopathy impairs fitness to drive. Hepatology **39**: 739-745, 2004.
6. Kooka Y, Sawara K, Endo R, Kato A, Suzuki K, Takikawa Y. Brain metabolism in minimal hepatic encephalopathy assessed by 3.0-Tesla magnetic resonance spectroscopy. Hepatol Res **46**: 269-276, 2016.
7. Kale RA, Gupta RK, Saraswat VA, et al. Demonstration of interstitial cerebral edema with diffusion tensor MR imaging in type C hepatic encephalopathy. Hepatology **43**: 698-706, 2006.
8. Srivastava A, Chaturvedi S, Gupta RK, et al. Minimal hepatic encephalopathy in children with chronic liver disease: prevalence, pathogenesis and magnetic resonance-based diagnosis. J Hepatol **66**: 528-536, 2017.
9. Qi R, Zhang LJ, Zhong J, et al. Grey and white matter abnormalities in minimal hepatic encephalopathy: a study combining voxel-based morphometry and tract-based spatial statistics. Eur Radiol **23**: 3370-3378, 2013.
10. Jensen JH, Helpern JA, Ramani A, Lu H, Kaczynski K. Diffusional kurtosis imaging: the quantification of non-gaussian water diffusion by means of magnetic resonance imaging. Magn Reson Med **53**: 1432-1440, 2005.
11. Ito K, Ohtsuka C, Yoshioka K, et al. Differential diagnosis of parkinsonism by a combined use of diffusion kurtosis imaging and quantitative susceptibility mapping. Neuroradiology **59**: 759-769, 2017.
12. Umesh Rudrapatna S, Wieloch T, Beirup K, et al. Can diffusion kurtosis imaging improve the sensitivity and specificity of detecting microstructural alterations in brain tissue chronically after experimental stroke? Comparisons with diffusion tensor imaging and histology. Neuroimage **97**: 363-373, 2014.
13. Marrale M, Collura G, Brai M, et al. Physics, Techniques and review of neuroradiological applications of diffusion kurtosis imaging (DKI). Clin Neuroradiol **26**: 391-403, 2016.
14. Wang JJ, Lin WY, Lu CS, et al. Parkinson disease: diagnostic utility of diffusion kurtosis imaging. Radiology **261**: 210-217, 2011.
15. Bester M, Jensen JH, Babb JS, et al. Non-Gaussian diffusion MRI of gray matter is associated with cognitive impairment in multiple sclerosis. Mult Scler **21**: 935-944, 2015.
16. Ito K, Kudo M, Sasaki M, et al. Detection of changes in the periaqueductal gray matter of patients with episodic migraine using quantitative diffusion kurtosis imaging: preliminary findings. Neuroradiology **58**: 115-120, 2016.
17. Kumar R, Gupta RK, Elderkin-Thompson V, et al. Voxel-based diffusion tensor magnetic resonance imaging evaluation of low-grade hepatic encephalopathy. J Magn Reson Imaging **27**: 1061-1068, 2008.
18. Qi R, Xu Q, Zhang LJ, et al. Structural and functional abnormalities of default mode network in minimal hepatic encephalopathy: a study combining DTI and fMRI. PLoS One **7**: e41376, 2012.
19. Chen HJ, Liu PF, Chen QF, Shi HB. Brain microstructural abnormalities in patients with cirrhosis without overt hepatic encephalopathy: a voxel-based diffusion kurtosis imaging study. AJR Am J Roentgenol **209**: 1128-1135, 2017.
20. Kawaguchi T, Konishi M, Kato A, et al. Updating the neuropsychological test system in Japan for the elderly and in a modern touch screen tablet society by resetting the cut-off values. Hepatol Res **47**: 1335-1339, 2017.
21. Yokosawa S, Sasaki M, Bito Y, et al. Optimization of scan parameters to reduce acquisition time for diffusion kurtosis imaging at 1.5T. Magn Reson Med Sci **15**: 41-48, 2016.
22. Ito K, Sasaki M, Ohtsuka C, et al. Differentiation among parkinsonisms using quantitative diffusion kurtosis imaging. Neuroreport **26**: 267-272, 2015.
23. Smith SM, Jenkinson M, Johansen-Berg H, et al. Tract-based spatial statistics: voxelwise analysis of multi-subject diffusion data. Neuroimage **31**: 1487-1505, 2006.
24. Hanai T, Shiraki M, Watanabe S, et al. Sarcopenia predicts minimal hepatic encephalopathy in patients with liver cirrhosis. Hepatol Res **47**: 1359-1367, 2017.
25. Shiraki M, Shimizu M, Moriwaki H, Okita K, Koike K. Carnitine dynamics and their effects on hyperammonemia in cirrhotic Japanese patients. Hepatol Res **47**: 321-327, 2017.
26. Suzuki K, Endo R, Takikawa Y, et al. Efficacy and safety of rifaximin in Japanese patients with hepatic encephalopathy: a phase II/III, multicenter, randomized, evaluator-blinded, active-controlled trial and a phase III, multicenter, open trial. Hepatol Res **48**: 411-423, 2018.
27. Li Y, Liu H, Yang J, Tian X, Yang H, Geng Z. Combining arterial-spin labeling with functional magnetic resonance imaging measurement for characterizing patients with minimal hepatic encephalopathy. Hepatol Res **47**: 862-871, 2017.
28. Fields RD, Stevens-Graham B. Neuroscience - New insights into neuron-glia communication. Science **298**: 556-562, 2002.